ELSEVIER

Lead telluride as a thermoelectric material for thermoelectric power generation

Z.H. Dughaish*

Department of Physics, Material Research Group, College of Science, King Saud University, P.O. Box 2455, Riyadh 11451, Saudi Arabia

Abstract

The specialized applications of thermoelectric generators are very successful and have motivated a search for materials with an improved figure of merit Z, and also for materials which operate at elevated temperatures. Lead telluride, PbTe, is an intermediate thermoelectric power generator. Its maximum operating temperature is 900 K. PbTe has a high melting point, good chemical stability, low vapor pressure and good chemical strength in addition to high figure of merit Z. Recently, research in thermoelectricity aims to obtain new improved materials for autonomous sources of electrical power in specialized medical, terrestial and space applications and to obtain an unconventional energy source after the oil crises of 1974. Although the efficiency of thermoelectric generators is rather low, typically $\sim 5\%$, the other advantages, such as compactness, silent, reliability, long life, and long period of operation without attention, led to a wide range of applications. PbTe thermoelectric generators have been widely used by the US army, in space crafts to provide onboard power, and in pacemakers batteries. The general physical properties of lead telluride and factors affecting the figure of merit have been reviewed. Various possibilities of improving the figure of merit of the material have been given, including effect of grain size on reducing the lattice thermal conductivity λ_L. Comparison of some transport properties of lead telluride with other thermoelectric materials and procedures of preparing compacts with transport properties very close to the single crystal values from PbTe powder by cold and hot-pressing techniques are discussed. © 2002 Elsevier Science B.V. All rights reserved.

PACS: 0720; 7220; 7220P; 7215J; 7430E; 7430F; 7280

Keywords: Transport properties; Seebeck coefficient; Electrical conductivity; Thermal conductivity; Lattice thermal conductivity; Electronic thermal conductivity; Lead telluride; Figure of merit; Thermoelectrics

1. Introduction

1.1. The thermoelectric phenomena

The three basic thermoelectric effects are the Seebeck effect, the Peltier effect, and the Thomson effect. These effects underlie the conversion of heat energy into electrical energy or vice versa. When a steady temperature gradient is maintained along a finite conductor, the free carriers at the hot end will have greater kinetic energy and tend to diffuse to the cold end. The accumulation of charge results in a back electromotive force (e.m.f) which opposes a further flow of charge. The Seebeck voltage is the open circuit voltage when no current

*Tel.: +966-1-47-69825; fax: +966-1-4673656.
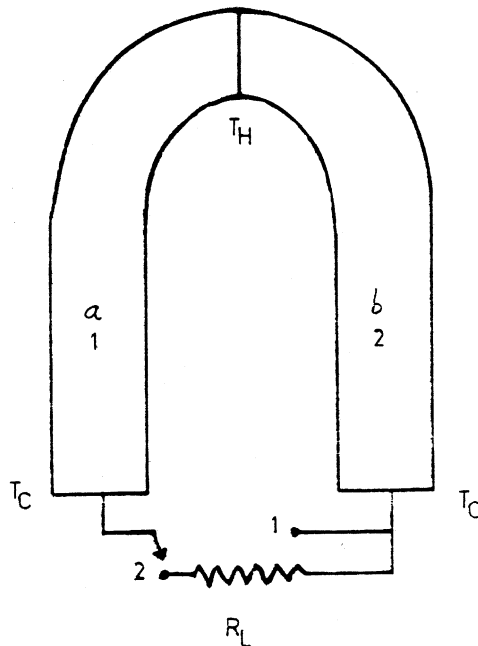
E-mail address: zhdalmas@ksu.edu.sa (Z.H. Dughaish).

Fig. 1. The Seebeck effect.

flows. If the junction of two dissimilar conductors a and b (Fig. 1) are maintained at two different temperatures T_H and T_C, where $T_H > T_C$, an open circuit potential difference is developed:

$$V = a_{ab}(T_H - T_C).$$

The Seebeck coefficient of the junction between two materials a and b is the same as the difference between the two absolute coefficients [1]:

$$\alpha_{ab} = \alpha_a - \alpha_b,$$

where α_a and α_b are the absolute Seebeck coefficients of the two materials a and b.

Thermocouples formed from two dissimilar conductors are used to measure temperature by thermoelectric generation of electricity from heat. Metal alloy thermocouples are also in use. Most metals possess Seebeck coefficients of $10\,\mu V\,K^{-1}$ or less, but semiconductor materials are promising in constructing the thermocouples because they have Seebeck coefficients in excess of $100\,\mu V\,K^{-1}$.

Good thermoelectric materials must have large Seebeck coefficients, high electrical conductivities and low thermal conductivities to retain the heat at the junction and to reduce the heat transfer losses. These requirements are summarized in what is called the figure of merit Z [2]:

$$Z = \frac{\alpha^2 \sigma}{\lambda}, \tag{1}$$

where α is the Seebeck coefficient, σ the electrical conductivity, and λ the thermal conductivity.

In the late 1950s realization that devices based upon the thermoelectric effect could have possible military applications [3,4] resulted in a tremendous experimental survey of semiconductor materials which led to the discovery of some semiconductor materials having Z-values higher than metals or metal alloys.

Recently, research in thermoelectricity aims to obtain new improved materials for autonomous sources of electrical power in specialized medical, terrestrial and space applications and to obtain an unconventional energy source after the oil crises of 1974 [5,6]. Large-scale thermoelectric generation of electricity requires the production of substantial amounts of semiconductor materials, accompanied by a significant improvement in the material figure of merit.

1.2. Theory of thermoelectric power generator

The theory of thermoelectric power generating devices has been discussed in a number of books [1,2,7,8,75] and review articles [9–13].

A thermoelectric power generator consists of many thermocouples. A thermocouple produces low voltage and high current. Thus, to obtain high voltages, a number of thermocouples are connected electrically in series and thermally in parallel to form a module. The module is heated at one end (hot side) and a temperature gradient was maintained with respect to the other end (cold side) as shown in Fig. 2.

The equation that describes this phenomenon may be written as

$$Q_{\lambda'} = \lambda'(T_H - T_C). \tag{2}$$

$Q_{\lambda'}$ is the conducted heat and λ' the total thermal conductance of the thermocouple.
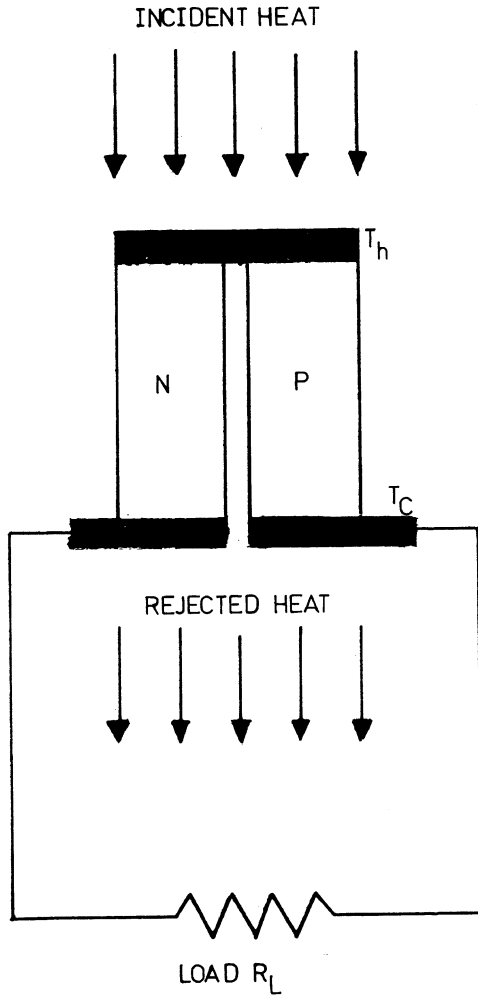
INCIDENT HEAT

Fig. 2. Typical thermocouple configuration. N,P: thermocouple arms.

In the case of semiconductors, each thermocouple consists of an n- and p-type arms (thermoelement) joined at a junction. If l is the length of the thermoelements and A is the cross sectional area, then λ' is given by

$$\lambda' = \frac{1}{l(A_n \lambda_n + A_p \lambda_p)}. \tag{3}$$

The temperature difference across the thermocouple sets up a Seebeck voltage across the thermoelements. The open circuit potential difference (V) developed at the terminals may be written as

$$V = \alpha_{pn} \Delta T, \tag{4}$$

where α_{pn} is the combined Seebeck coefficient of the two thermoelements and is given by

$$\alpha_{pn} = \alpha_p - \alpha_n. \tag{5}$$

When a load R_L is connected across the terminals of the thermocouple, a thermoelectric current I passes in the outer circuit and is given by

$$I = \alpha_{pn} \Delta T / [R + R_L], \tag{6}$$

where R is the internal resistance of the thermocouple and is given by [14]

$$R = l\left(\frac{\rho_n}{A_n} + \frac{\rho_p}{A_p}\right), \tag{7}$$

where ρ_n and ρ_p are the electrical resistivities of the n and p thermoelements, respectively.

The passage of the thermoelectric current across the junction results in heat generation or absorption as a result of the Peltier effect. The quantity of heat Q_P generated (or absorbed) is given by

$$Q_P = \pi I, \tag{8}$$

where π is the Peltier coefficient.

The Joule heat Q_J due to the passage of the current I in the circuit is given by

$$Q_J = I^2 R. \tag{9}$$

It has been shown [15] that, to a first approximation, one-half of the Joule heat generated at the junction is transported to each of the thermocouple elements.

A detailed heat balance at the junction of the thermocouple may be given as

$$Q_H = Q_{\lambda'} + Q_H - \tfrac{1}{2} Q_J. \tag{10}$$

Similarly, the total heat rejected at the junction, Q_C, may be given as

$$Q_C = Q_{\lambda'} + (Q_P)_C + \tfrac{1}{2} Q_J. \tag{11}$$

Applying the energy conservation laws, we get

$$Q_H = Q_C + I^2 R_L. \tag{12}$$

1.3. The efficiency of thermoelectric power generator

The efficiency of the generator is defined as

$$\eta = \frac{\text{Electrical energy generated at the load } R_\text{L}}{\text{Heat energy input at the hot junction}}$$

$$= \frac{E}{Q_\text{H}}. \qquad (13)$$

From the above equations, η may be expressed as

$$\eta = \frac{I^2 R_\text{L}}{\lambda'(T_\text{H} - T_\text{C})} + \pi I - \frac{1}{2} I^2. \qquad (14)$$

For a fixed value of $T_\text{H} - T_\text{C}$ and a maximum power output, the efficiency η_p is given by [1]

$$\eta = \frac{(T_\text{H} - T_\text{C})}{\frac{3}{2} T_\text{H} + T_\text{C} + 4/Z_\text{C}}, \qquad (15)$$

$$\eta_0 = \frac{(T_\text{H} - T_\text{C})(1 + Z_\text{C}\bar{T})^{1/2} - 1}{T_\text{H}(1 + Z_\text{C}\bar{T})^{1/2} + T_\text{C}/T_\text{H}}, \qquad (16)$$

where $\bar{T} = (T_\text{H} - T_\text{C})/2$. For good thermoelectric materials $Z_\text{C}\bar{T} \sim 1$. For $Z_\text{C}\bar{T} \ll 1$, η_0 is approximated as

$$\eta_0 \cong \tfrac{1}{4} Z_\text{C} \Delta T, \qquad (17)$$

where Z_C is called the figure of merit of the couple and is given by

$$Z_\text{C} = \frac{\alpha_\text{ab}^2}{R\lambda'} \qquad (18)$$

and α_ab is the Seebeck coefficient for the junction.

If the two arms of the thermocouple are of identical geometry to minimize heat absorption, then

$$Z_\text{C} = \frac{(\alpha_\text{p} - \alpha_\text{n})^2}{\left\{ (\lambda_\text{p}/\sigma_\text{p})^{1/2} + (\lambda_\text{n}/\sigma_\text{n})^{1/2} \right\}^2}. \qquad (19)$$

In practice, the two arms have similar material constants and may be considered as a single material; the figure of merit is given by

$$Z = \frac{\alpha^2 \sigma}{\lambda}, \qquad (20)$$

where σ is the electrical conductivity.

Assuming $T_\text{C} = 300$ K, η_0 is plotted against T for a range values of Z as shown in Fig. 3 [11]. Thus, for maximum efficiency, the factor ZT
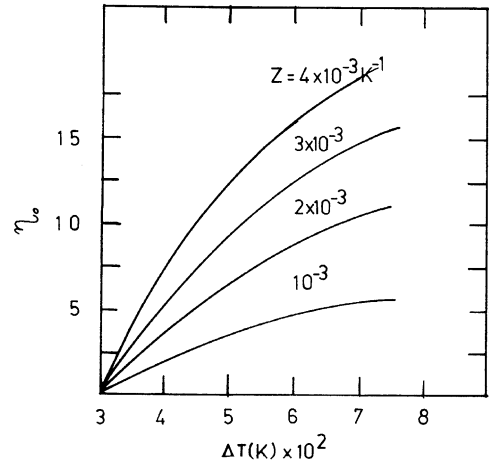

Fig. 3. Efficiency η_0 of a thermoelectric generator as a function of temperature for a cold junction temperature of 300 K [11].

should be maximized, that is, Z should have high values over as wide range of temperature as possible. Z is optimized at a carrier concentration of 10^{25}–10^{24} m^{-3}. From Eq. (20), the unit of Z is K^{-1}, and since Z may vary with temperature, ZT is a useful non-dimensional figure of merit.

In a two-stage thermoelectric module, the conversion efficiency is about 13.5%, while it is about 40% for a central power station [16].

The specialized applications of thermoelectric generators are very successful and have motivated a search for materials with an improved figure of merit, Z, and also for materials which operate at increased temperatures.

1.4. Factors affecting the figure of merit Z

The figure of merit as defined by Eq. (20) embodies three parameters: the Seebeck coefficient α, the electrical conductivity σ, and the total thermal conductivity λ. All three are functions of the carrier concentration. Fig. 4 shows the dependence of these parameters on the carrier concentration. From this figure, it is seen that the figure of merit reaches its maximum value around a carrier concentration of 10^{26} m^{-3}, which corresponds to heavily doped or near degenerate semiconductors. The precise carrier concentration to maximize Z depends on temperature and on the
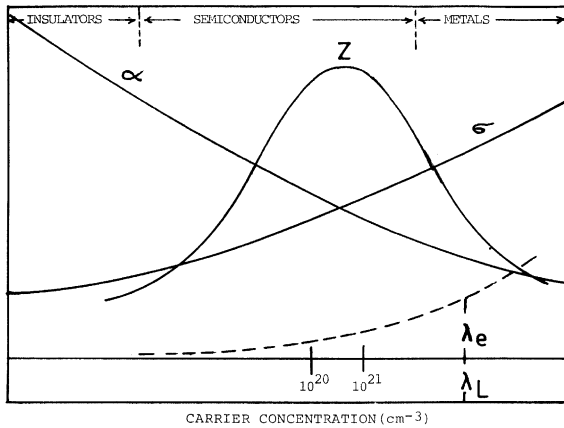
Fig. 4. Dependence of Seebeck coefficient α, electrical conductivity σ and thermal conductivity (λ_e, λ_L) on the concentration of free carriers.

specific semiconductor. Thus, it is difficult to increase the electrical conductivity of the material by increasing the carrier concentration in order to maximize Z without affecting the other parameters α and λ.

For metals and metal alloys the ratio λ/σ is constant and it is directly proportional to the temperature. From The Wiedemann–Franz law at not very low temperature ($T > \theta_D$, where θ_D is the Debye temperature) this ratio is given by [17]

$$\frac{\lambda}{\sigma} = \frac{\pi^2}{3}\left(\frac{k}{e}\right)^2 T, \tag{21}$$

where k is the Boltzman constant, and e is the charge of the electron.

The Lorenz number L is defined as

$$L = \frac{\lambda}{\sigma T} = \frac{\pi^2}{3}\left(\frac{k}{e}\right)^2. \tag{22}$$

Semiconductors have λ/σ greater than that of metals owing to their poorer electrical conductivity, and posses Seebeck coefficients in excess of $100\,\mu\text{V K}^{-1}$ while most metals have Seebeck coefficients of $10\,\mu\text{V K}^{-1}$ or less.

In the general case, the Wiedemann–Franz law for semiconductors has the following form [2]:

$$\frac{\lambda}{\sigma} = (s + 2)\left(\frac{k}{e}\right)^2 T, \tag{23}$$

where s is the scattering parameter defined as

$$l = l_0(T)E^s, \tag{24}$$

where l is the free path length (mean free path) of the carriers, E is the carrier energy, and s is a constant which depends upon the scattering mechanism: $s = -\frac{1}{2}$ for acoustic phonon scattering; $s = +\frac{1}{2}$ for optical phonon scattering (alloy disorder scattering); and $s = \frac{3}{2}$ for ionized impurity scattering.

Ioffe [18] has shown that the ratio λ/σ can be decreased if the thermoelectric material is alloyed with an isomorphous element or compound.

Thermal conductivity in semiconductors is mainly due to the lattice contribution λ_L, while in heavily doped materials the electronic or hole contribution λ_e may become significant. In the range of intrinsic conduction the bipolar contribution λ_b to thermal conductivity must be taken into account. There are other contributions by photons to the conductivity λ_{photon}, but to good approximation, the total thermal conductivity is expressed as

$$\lambda_t = \lambda_L + \lambda_e + \lambda_b. \tag{25}$$

For a unipolar material where only electrons or holes predominate, the total thermal conductivity λ_t may be written as

$$\lambda_t = \lambda_e + \lambda_L, \tag{26}$$

where λ_e and λ_L are the electronic and lattice or phonon thermal conductivity, respectively.

1.5. The dimensionless figure of merit

The dimensionless figure of merit ZT can be expressed as [14]

$$ZT = (s + 1)F_s(\xi)\left(\frac{s+2}{s+1}\right)^2 \frac{\left\{\dfrac{F_{s+1}(\xi)}{F_s(\xi)} - \xi\right\}^2}{\pi^{1/2}(s+1)\dfrac{F_s(\xi)}{A'F_{1/2}(\xi)} + (s+3)F_{s+2}(\xi) - \dfrac{(s+2)^2 F_{s+2}^2(\xi)}{(s+1)F_s(\xi)}}, \tag{27}$$

Table 1
Important material parameters [30]

Material	C_{11} (N m^{-1})	ε_1	λ_{L} (W m^{-1} K^{-1})	N_{V}	E_{g} (eV)	ε_0	ε_∞
PbTe	1.39×10^{11}	24	1.7	4	0.32	400	38
InAs	1.0×10^{11}	5.8	29	1	0.46	14.54	11.74
InSb	0.67×10^{11}	7.2	15	1	0.165	17.64	15.75

where F_s is the Fermi integral defined as

$$F_s(\xi) = \int_0^\infty \frac{x \, \mathrm{d}x}{\mathrm{e}^{x-\xi} + 1}.$$

$\xi (= E_{\mathrm{F}}/kT)$ is the reduced (dimensionless) Fermi level, and A' is a dimensionless material parameter:

$$A' = \frac{2(\pi k)^{3/2} k^2 A''}{eh^3} \tag{28}$$

and

$$A'' = T^{5/2} m^{*3/2} \frac{\mu}{\lambda_{\mathrm{L}}}. \tag{29}$$

ZT increases monotonically as A', and subsequently A'' increases. To obtain large values of A'', $m^{*3/2}$ should be as large as possible and λ_{L} should be small.

The figure of merit, in its dimensionless form, for a single band conduction model, is expressed by [16,23]

$$ZT = \frac{\alpha'^2 \sigma'}{1 + \sigma' L'} = \frac{\alpha'^2 \sigma'}{1 + \lambda_{\mathrm{e}}/\lambda_{\mathrm{L}}}, \tag{30}$$

where α' and σ' are the reduced Seebeck coefficient and electrical conductivity, respectively. They are defined as

$$\alpha' = +\left(\frac{e}{k}\right)\alpha, \tag{31}$$

$$\sigma' = \left(\frac{k}{e}\right)^2 \frac{T}{\lambda_{\mathrm{L}}}. \tag{32}$$

Important physical parameters of PbTe, InSb and InAs are given in Table 1. From the table, it is clear that PbTe is the only material which has $N_{\mathrm{V}} = 4$; i.e., inter-valley scattering must be considered while the other two materials have $N_{\mathrm{V}} = 1$. Calculated values of $\lambda_{\mathrm{e}}/\lambda_{\mathrm{L}}$ and ξ according to this procedure are shown in Figs. 5 and 6 as functions of ξ for parabolic and non-parabolic bands for
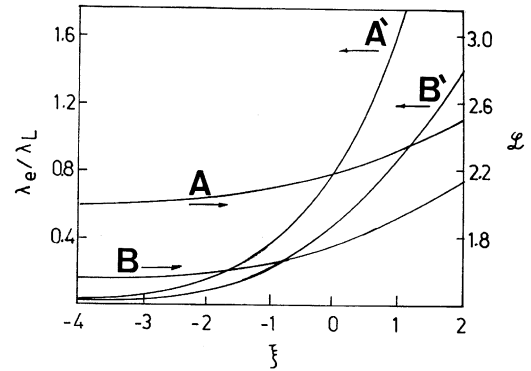

Fig. 5. The ratio $\lambda_{\mathrm{e}}/\lambda_{\mathrm{L}}$ and the Lorenz factor L, as a function of the reduced Fermi energy ξ for PbTe at 300 K. Acoustic phonon scattering without inter-valley scattering [30]. Curves A and B refer to parabolic and non-parabolic bands, respectively.
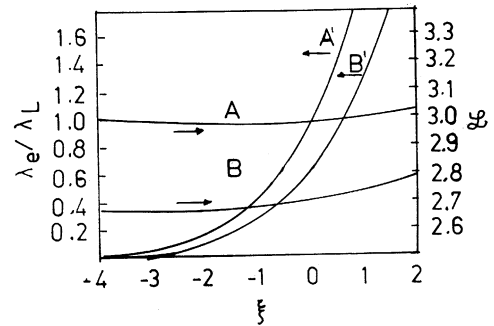

Fig. 6. The ratio $\lambda_{\mathrm{e}}/\lambda_{\mathrm{L}}$ and the Lorenz factor L, as a function of the reduced Fermi energy ξ for PbTe at 300 K. Polar optical scattering [30]. Curves A and B refer to parabolic and non-parabolic bands, respectively.

PbTe at 300 K [30]. Scattering of carriers by acoustic and optical modes has been shown. From these figures it is clear that the effect of non-parabolicity has reduced the ratio $\lambda_{\mathrm{e}}/\lambda_{\mathrm{L}}$ corresponding to a particular values of ξ. ε_0 and ε_∞ are

Table 2
The ratio λ_e/λ_L for lead telluride corresponding to ξ_{opt} at different temperatures and appropriate to parabolic and non-parabolic energy bands: acoustic phonon scattering [30]

T (K)	ξ_{opt}	λ_e/λ_L (parabolic band) $\beta_g = 0$	λ_e/λ_L (non-parabolic band) $\beta_g = 0.08$, fixed	λ_e/λ_L (non-parabolic band) $\beta_g = 1/\xi_g$
300	−0.75	0.50	0.27	0.25 (0.15)
500	−0.90	0.70	0.35	0.30
700	−1.20	1.00	0.50	0.40
900	−1.30	1.25	0.65	0.50

Fig. 8. Variation of the Lorenz factor L' with temperature for PbTe at different carrier concentrations. Curves: A, $3 \times 10^{25}\,\text{m}^{-3}$, B, $10^{25}\,\text{m}^{-3}$, C, $5 \times 10^{24}\,\text{m}^{-3}$, D, $10^{24}\,\text{m}^{-3}$, and E, $2 \times 10^{23}\,\text{m}^{-3}$ [16].

Fig. 7. The ratio λ_e/λ_L, as a function of the reduced Fermi energy ξ or PbTe at different temperatures. A non-parabolic energy band is considered with $\beta_g = kT/E_g$; acoustic phonon scattering. Curves: A at 300 K, B at 500 K, C at 700 K, and D at 900 K [30].

the static dielectric constant and the dielectric constant of high frequency, ε_l is the chemical potential, and C_{11} is the elastic constant related to the average sound velocity.

Table 2 represents the ratio λ_e/λ_L for PbTe corresponding to ξ_{opt} at different temperatures for parabolic and non-parabolic energy bands; scattering of carriers has been taken as due to acoustic phonons only [30].

Fig. 7 shows the ratio λ_e/λ_L as a function of ξ for PbTe at different temperatures [30]. Fig. 8 shows the Lorenz factor L' as a function of temperature and carrier concentrations [16].
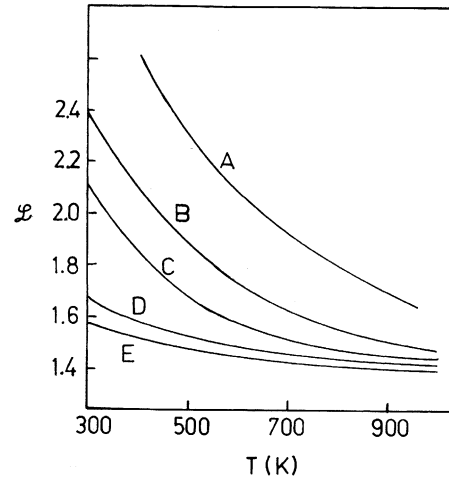
1.6. Theoretical models for analysis of the dimensionless figure of merit

For narrow band-gap semiconductors such as PbTe and Si–Ge alloys, the thermal conductivity is strongly influenced by the non-parabolic nature of the energy bands. Bhandari and Rowe [19] have produced a detailed theoretical analysis of the figure of merit for a model system which was a close approximation to silicon–germanium alloys.

An improved theoretical model has been used to analyze the high-temperature thermal conductivity of doped n-type PbTe in terms of separate contributions from electrons and phonons. This model takes into consideration that at high carrier concentration, carrier scattering mechanism plays an important role in modifying the thermal conductivity and both acoustic phonon and polar optical scattering must be included in the analysis of the experimental data. Effect of the multi-valleys in the energy band structure in increasing the figure of merit and other effects are also taken into consideration of the system as follows:

1. *Effect of the presence of large number of valleys in the energy band structure*: They showed that the presence of a large number of valleys may

help in attaining a high figure of merit. However, the presence of many valleys may lead to inter-valley scattering which effectively offsets any improvement in the figure of merit. The net result will probably be slightly higher than the single-valley case.

2. *Effect of various scattering mechanisms*: Mixed scattering of ionized impurity scattering and lattice scattering as applied to a single-valley model showed a closer agreement of ZT-values with the experimental values.

3. *Effect of hot-press sintering on the lattice thermal conductivity λ_L*: Hot-pressing the thermoelectric materials has the possibility of reducing the lattice thermal conductivity λ_L.

In alloys where the constituent elements have large differences in atomic masses, short wavelength phonons are scattered by the alloy disorder, the heat being conducted by phonons of long wavelength. These phonons are scattered by grain boundaries [20–22].

2. Lead telluride as a thermoelectric material

Most of the widely used thermoelectric semiconductor materials are based upon bismuth telluride, lead telluride, silicon–germanium alloys, and more. Recently, boron-based and boron–carbon materials are promising materials for high-temperature thermoelectric generation. Each material has its own range of useful operating temperatures and the figure of merit of each material differs considerably.

Fig. 9 shows the variation of the figure of merit Z of the most common thermoelectric materials versus temperature [12]. Table 3 shows the maximum operating temperature, range of operating temperatures, figure of merit, and the maximum efficiency of some thermoelectric materials [35,36,75].

It is apparent from Eq. (17) that the extent of the useful range of operating temperature is as important to the performance of the thermocouple as is the figure of merit. Fig. 10 shows the
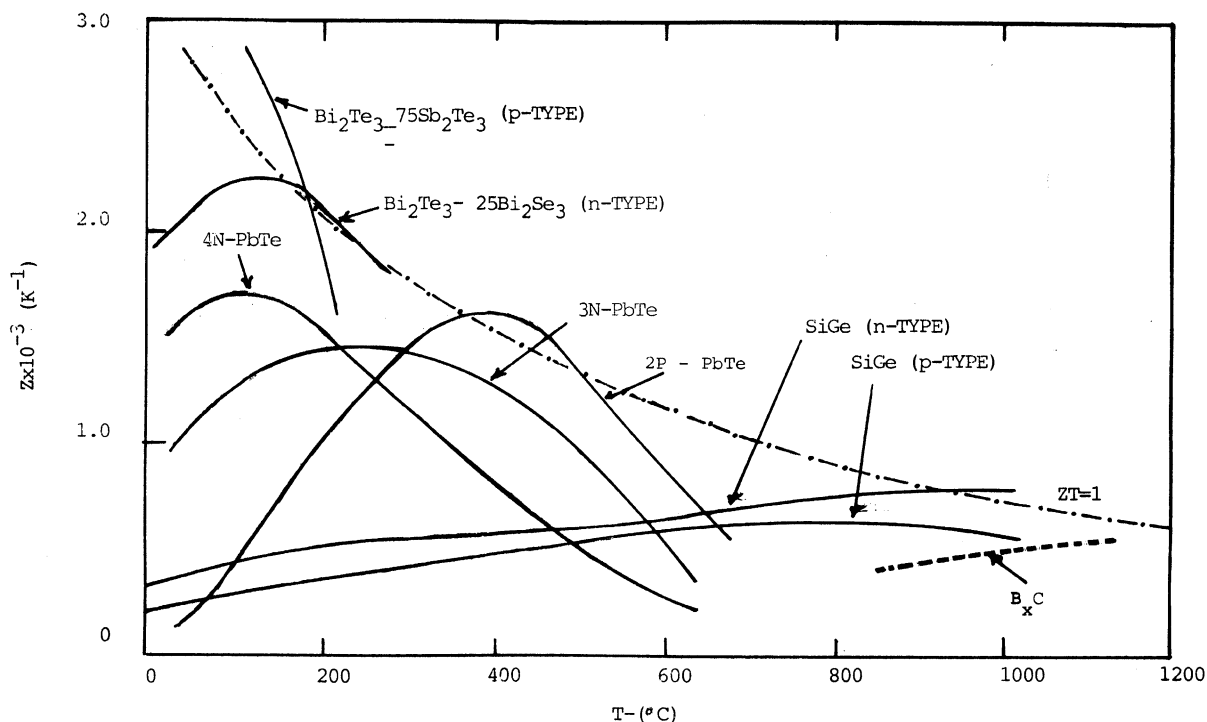

Fig. 9. Figure of merit of the most common thermoelectric materials as a function of temperature [12].

Table 3
The maximum operating temperature, range of operating temperatures, figure of merit, and the maximum efficiency of some thermoelectric materials [35,36]

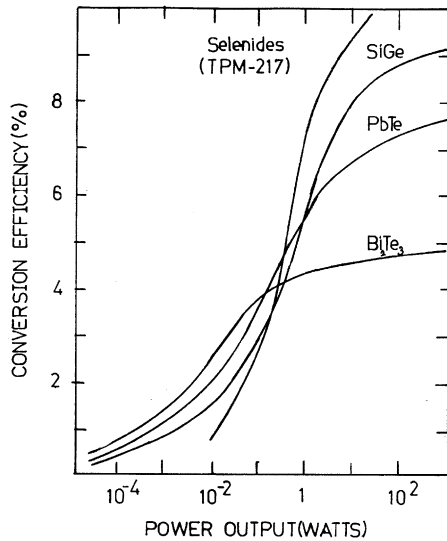| Material	Max. temp. (K)	ΔT ($T_C = 450$ K)	Average Z (K^{-1})	Max. efficiency $\eta_0 = \frac{1}{4} Z \Delta T$
Bismuth telluride (Bi$_2$Te$_3$)	550	100	0.0018	0.04
Lead telluride (PbTe)	900	450	0.0010	0.11
Silicon–germanium (Si–Ge)	1400	850	0.0070	0.15
Boron-based material	1300	950	0.00070	0.015

Fig. 10. Conversion efficiency as a function of electrical power output [13,35,36].

conversion efficiency of bismuth telluride, lead telluride, selenides and silicon–germanium alloys, as a function of electrical power output [15,35,36].

Although the efficiency of thermoelectric generators at present is rather low, typically $\sim 5\%$, the other advantages, such as compactness, silent, reliability, long life, and long periods of operation without attention, led to a wide range of applications. PbTe thermoelectric generators have been widely used by the US army [3,4], in space crafts [27–30] to provide onboard power, and in pace-makers batteries.

Lead telluride is considered as an intermediate thermoelectric material. Its maximum operating temperature is 900 K. PbTe has a high melting point, good chemical stability, low vapor pressure and good chemical strength in addition to high figure of merit.

2.1. Doping of PbTe

Lead telluride, PbTe, has a rocksalt structure (face-centered cubic (FCC)). PbTe can be n- or p-type material as a result of departure from stoichiometry, (Pb-rich PbTe is n-type, while Te-rich PbTe is p-type). To produce values of the Seebeck coefficient of $+200\,\mu$V K^{-1}, doping is necessary.

The electrical properties of PbTe are greatly affected by adding foreign atoms to the PbTe lattice. Halogens may be used via PbCl$_2$, PbBr$_2$ or PbI$_2$ to produce donor centers. Other n-type doping agents such as Bi$_2$Te$_3$, TaTe$_2$, MnTe$_2$, are added to PbTe, they substitute for Pb and thus create uncharged vacant Pb-sites. These vacant sites are subsequently filled by atoms from the lead excess. Because the valence electrons of these vacant atoms are not involved in chemical bonding, they diffuse through the crystal. The donor concentration induced by the foreign species is found to be independent of heat treatment. Alkali acceptor agents in lead telluride are discussed by Kovalchik et al. [38], Borisova [39] and Rustamov et al. [40].

p-Type doping agents such as Na$_2$Te, K$_2$Te, Ag$_2$Te substitute for Te and create vacant uncharged Te sites. These sites are filled by Te atoms which are ionized to create additional positive holes. The free electron (n-type) or hole concentration (p-type) in PbTe is the sum of the electrons or holes originating from Pb or Te in solution plus the electrons or holes introduced by the donor or acceptor species.

All foreign molecular species (agents) effective as donors or acceptors are known as negative and positive promoters, respectively. Fig. 11 shows the room temperature resistivity of positive promoters and Fig. 12 shows the room temperature resistivity
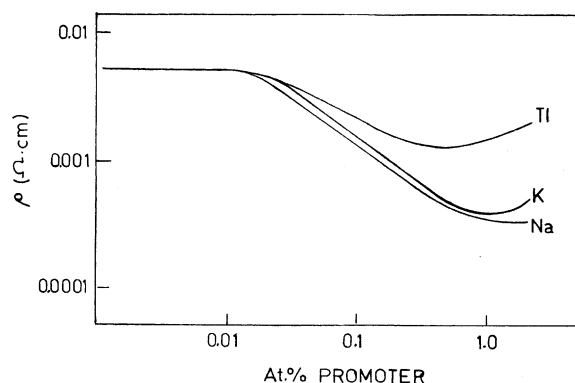

Fig. 11. Room temperature electrical resistivity of PbTe p-type doping curves of positive promoters.
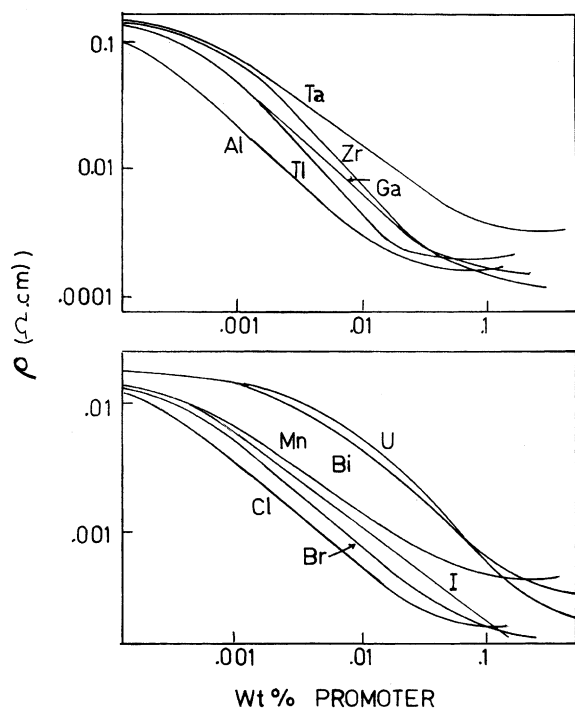

Fig. 12. Room temperature electrical resistivity of PbTe n-type doping curves of negative promoters.

of negative promoters as a function of promoters concentration.

2.2. Transport properties of PbTe

The electrical conductivity and the Seebeck coefficient of PbTe vary with temperature for various doping levels as shown in Figs. 13 and 14 [12]. The figure of merit of PbTe changes with temperature and for various doping levels as shown in Fig. 15 and Fig. 16 for n-type and p-type PbTe, respectively [12]. The temperature dependence of mobility for n-type PbTe at high temperatures is shown in Fig. 17 (theoretical curves and experimental data) [25].

Various properties of PbTe have been discussed in detail by Ravich et al. [24,25] and Scanlon [26]. PbTe has been used as a thermoelectric generator in many applications where conventional power sources are unsuitable.

2.3. Improving the figure of merit

It has been shown [20,31] that the figure of merit can be improved by reducing the lattice thermal conductivity λ_L which contributes about 75% of the total thermal conductivity λ_t, provided the electrical properties of the thermoelectric material remain unaffected.

Attempts to improve the thermoelectric performance of these materials were made by decreasing the λ_L component of the thermal conductivity while maintaining the original values of α and σ. Phonon-grain boundary scattering has a significant effect in reducing the lattice thermal conductivity λ_L of semiconductor alloys when the phonon mean free path or wavelength is comparable to the grains dimensions without affecting α and σ [26].

Disorder scattering will be present in PbTe and its alloys due to mass differences of the atoms. This mass difference is smaller than that in the Si–Ge alloys, so smaller grain sizes than those in Si–Ge alloys will be required to get a significant reduction in λ_L.

Theoretical calculations indicated that a reduction of 7% in λ_L in optimally doped PbTe can be
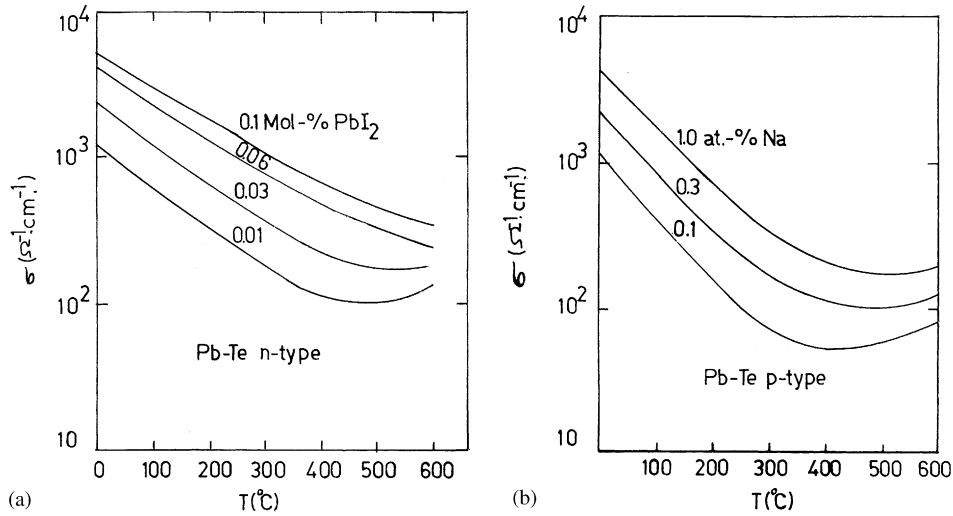
Fig. 13. (a) Electrical resistivity of n-PbTe as a function of temperature [12]. (b) Electrical resistivity of p-PbTe as a function of temperature [12].
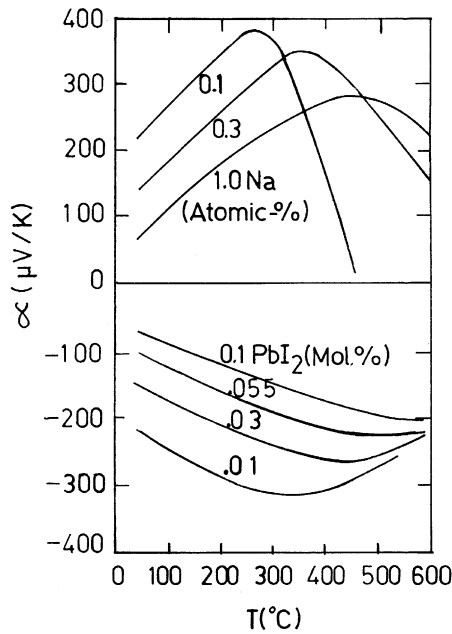

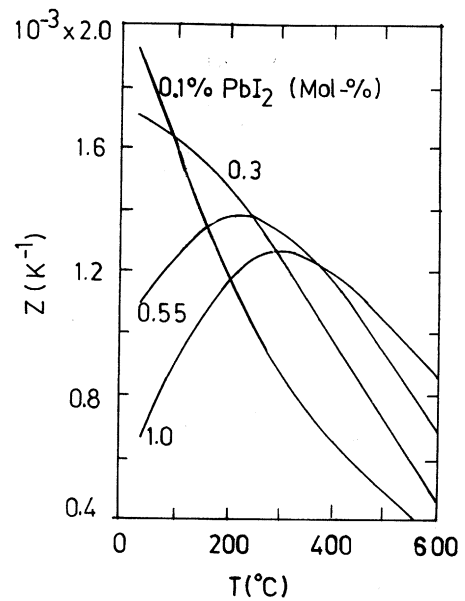Fig. 14. Seebeck coefficient of PbTe as a function of temperature [12].

Fig. 15. Figure of merit of n-PbTe as a function of temperature [12].

obtained with a mean grain size of the order of 0.5 μm [37].

Materials prepared by hot-pressing techniques hold out such a possibility of reducing the lattice

thermal conductivity by scattering of phonons at the grain boundaries. Grain boundary scattering of phonons is more pronounced in alloys where the atoms of the constituents have large differences in atomic masses. In Si–Ge alloys, the ratio
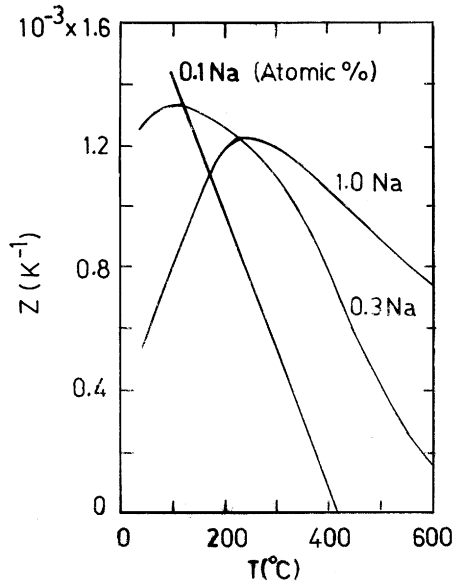
Fig. 16. Figure of merit of p-PbTe as a function of temperature [12].

Fig. 17. Hall mobility of electrons in PbTe from 500 to 80 K (theoretical curve and experimental data) [26].

between the atomic masses of Si and Ge is 0.387 while it is 0.616 for Te and Pb [34]. So, the lattice disorder scattering is less effective in PbTe than in Si–Ge alloys. Short wavelength phonons are scattered by alloy disorder, while the long wavelength phonons are effectively scattered at the grain boundaries.

Fine-grained hot-pressed silicon–germanium alloys show a reduction in lattice thermal conductivity compared with single crystal [13,19]. In heavily doped Si–Ge alloys of grain size $L < 5\,\mu m$, a reduction of 28% in lattice thermal conductivity has been reported [14,31].

Several researchers have discussed the control of heat conduction in nanostructures through phonon engineering, and nanoscale heat transfer in microelectronics [60], energy technology [61], and thermoelectric cooling in bulk and quantum-well semiconductors [62,63]. Recently, the thermoelectric properties of superlattices have been of considerable interest because of their potential as improved thermoelectric materials. Promising work [64–74] to increase the figure of merit of thermoelectric materials is carried on by using thin films and nanostructures instead of the bulk to
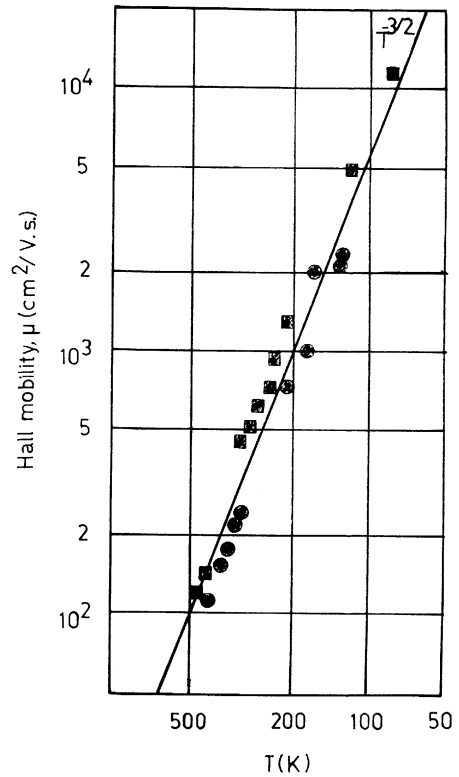
reduce the thermal conductivity via acoustical phonon confinement and interface scattering. It has been suggested that ZT in superlattices formed from quantum wells and quantum wires may be dramatically increased over those for bulk because of the increase of the electronic density of states that occurs in ideal two- and one-dimensional systems.

Hicks and Dresselhaus [64,65] have shown that the dimensionless figure of merit ZT of Bi_2Te_3 in a quantum-well structure has the potential to be increased by a factor of 13 over the bulk value. This large increase depends crucially on the material's highly anisotropic effective-mass tensor. To achieve this increase, the layers must be prepared in the $a_0 - c_0$ plane and the current must flow along the highest mobility a_0-axis. If the multi-layers are prepared perpendicular to the c_0-axis along the $a_0 - b_0$ plane, then there is still an

increase of a factor of 3 over the bulk value, provided the layers can be made 10 Å thick.

Harman et al. [66] reported a value of $Z_{2D}T > 1.2$ at room temperature for PbTe multiple quantum wells (MQWs). Fan et al. [63] have reported a reduction of over one order in the cross-plane thermal conductivity of $Si_{0.89}Ge_{0.10}C_{0.01}$ superlattice than that of Si.

Theoretical calculations of Hyldgaard and Mahan [68] predict in Si/Ge superlattices an order-of-magnitude high-temperature suppression in the ratio of the perpendicular thermal conductivity to the phonon relaxation time. Balandin and Wang [69,70] have predicted, from their numerical calculations, a decrease in the lattice thermal conductivity by an order of magnitude in a 100-Å-wide free-standing silicon quantum well at $T = 293-413$ K.

Dresselhaus et al. [71,72] have studied the nanostructured material and the quantum wires of bismuth (Bi). More recently, Kong et al. [73] reported the measurement of a factor of 7 enhancement of ZT relative to bulk Si for a Si/Ge superlattice. Khitun et al. [74] have studied the figure of merit of $Si_{1-x}Ge_x$ quantum wires rigorously taking into account spatial confinement of both electrons and phonons. A significant enhancement of ZT (order of magnitude) is predicted despite the decrease of the carrier mobility in very narrow quantum wires. The enhancement is mostly a result of the drop in the lattice thermal conductivity caused by the spatial confinement of acoustic phonons and the corresponding increase in phonon relaxation rates. The predicted increase is important for the anticipated applications of $Si_{1-x}Ge_x$ nanostructured materials for high-temperature thermoelectric devices.

2.4. Properties of lead telluride, PbTe

2.4.1. General properties

It is known that PbTe and the solid solutions based on it are promising materials for use in thermoelectric generation [2,38,39,47,49], laser industry and microelectronics [50–56]. PbTe is a semiconductor with an energy gap of 0.3 eV. Its crystal structure is FCC of lattice constant $a_0 = 6.5 + 0.02$ Å. The melting point of undoped

Table 4
Some physical properties of PbTe

Band gap	0.22 eV
Work function	4.1 eV
Melting point	1190 K
Density	8150 kg m^{-3}
Lattice constant	6.440 Å
Young's modulus	1.38×10^{11} N m^{-2}
Thermal expansion coefficient	18×10^{-6} K^{-1}
Activation energy	15×10^4 J mol^{-1}
Number of valleys N_v	4
Debye temperature θ_D	130 K
Specific heat	155 J kg^{-1} K^{-1}
Mobility μ_e	0.21 m^2 s^{-1} V^{-1}

PbTe is 1190 K for 50 at% Te and has a density of 8.15×10^3 kg m^{-3}. Some physical properties of PbTe are given in Table 4.

2.4.2. Sublimation of PbTe

PbTe sublimates at high temperature. There could be a change in stoichiometry due to the loss of the dopant or any of the constituents, which in turn alters the thermoelectric properties of the material. Consequent attempts to minimize the sublimate were reported. Killian [32] covered the specimens with sleeves of various annulus sizes. He found a reduction of 3552 in the weight loss rate for the annulus of 7×10^{-5} m compared with unsleeved (weight loss rate of 9.13×10^{-10} kg s^{-1} for unsleeved, and 2.57×10^{-13} kg s^{-1} for sleeved one with the annulus). Field and Bunde [33] predicted that the rate of sublimation of PbTe follows the following formula:

$$\Gamma = \frac{2\pi r_0 \gamma T^{1/2}}{P\eta} e^{-E_a/R_0 T}, \tag{33}$$

where Γ is the rate of sublimation (kg m^{-2} s^{-1}), r_0 is the radius of the specimen, γ is the proportionality constant, T is the absolute temperature, P is the surrounding gas pressure (N m^{-2}), E_a is the activation sublimation energy (J kg^{-1}), R_0 is the universal gas constant = 24.81 J kg^{-1} K^{-1}, and $\eta = 1$ for argon. They calculated the rate of sublimation based on a fixed sample radius of 0.318×10^{-2} m. For n-type PbTe, the calculated rate of sublimation at 873 K was 2.1×10^{-7} kg m^{-2} s^{-1} at 1.722×10^5 N m^{-2}. This rate ranged

from 9×10^{-8} kg m^{-2} s^{-1} at 673 K to 6×10^{-4} kg m^{-2} s^{-1} at 873 K in vacuum. For p-type PbTe, the rate of sublimation changed from 1.9×10^{-6} kg m^{-2} s^{-1} at 723 K to 7×10^{-3} kg m^{-2} s^{-1} at 873 K in vacuum. Recent studies [34,58] using positive cover gas pressure of inert argon gas in the range 1.38×10^{5}–3.79×10^{5} N m^{-2} showed that the rate of sublimation varied significantly with increasing cover gas pressure. It decreased from 9.69×10^{-6} kg m^{-2} s^{-1} at 1.722×10^{5} N m^{-2} to 4.52×10^{-6} kg m^{-2} s^{-1} at 3.79×10^{5} N m^{-2}; thus, a reduction of 50% in the rate of sublimation was achieved. A further reduction in the rate of sublimation could be achieved by applying higher gas pressures provided the equipment can withstand it.

2.4.3. Preparation of PbTe

PbTe has the phase diagram shown in Fig. 18 [8,9]. It has a single freezing point at 50:50 at% of Pb and Te concentrations and resembles a metal in this respect. PbTe is usually prepared from high-purity Pb and Te elemental components. It is customary to seal them inside an evacuated silica ampul. Large single crystals are prepared by a modified Bridgman–Stockbarger technique by traversing the charge inside a furnace with a large longitudinal temperature gradient. The furnace is

heated to a temperature above the melting point of PbTe (1190 K).

Large single crystals are also prepared by the zone melting technique. Homogeneous PbTe has also been prepared by isothermal cooling [34]. Fine-grained PbTe can be produced by quenching from the melt [34].

2.4.4. Preparation of PbTe compacts

2.4.4.1. Compacts from coarse powder. Coarse powder compacts are obtained by cold-pressing the powder at 6.97×10^{4} N followed by a two stage annealing procedure. First, the material is heated at 1033 K for 3 h, second, it is cooled down slowly inside the furnace to 703 K and kept constant at this temperature for 4 h. The furnace was switched off and the sample slowly cooled inside the furnace to room temperature [34,57].

2.4.4.2. Compacts from very fine powder. Preparing compacts from very fine powder was not easy. A suitable method is the hot-pressing technique employed in obtaining dense compacts. A three-stage annealing procedure should be followed to bring the transport properties of the hot-pressed compacts close to the single crystal values. Annealing at 873 K for 16 h, then annealing at 973 K for 8 h, and finally for 2 h at 1033 K, followed by quenching in ice-water bath [34,59]. Annealing at 1033 K must not proceed for more than 4 h, because of the decrease in densification which accompanies longer annealing periods.

The above-mentioned procedures should be followed to prepare the PbTe compacts with transport properties close to the single crystal values.

2.4.5. Effect of grain size on the reduction of the lattice thermal conductivity λ_{L}

In insulators, heat is transferred by phonons, while in metals heat is transported by both electrons and phonons; so the thermal conductivity λ can be expressed as

$$\lambda_{t} = \lambda_{e} + \lambda_{L}. \tag{34}$$

In most metals due to the great concentration of electrons $\lambda_{L} \sim 10^{-2} \lambda_{e}$, so λ_{L} can be neglected.
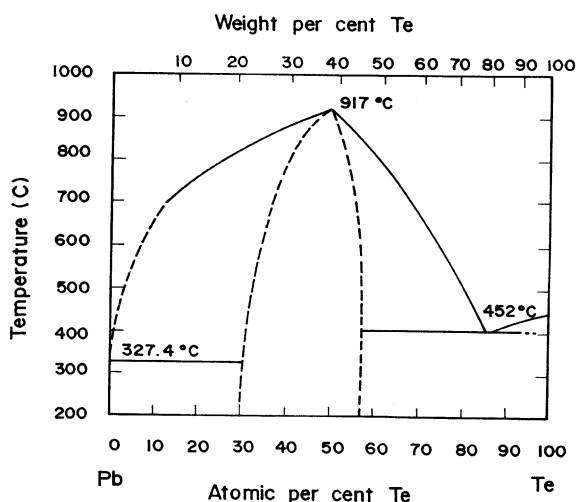
Fig. 18. Phase diagram of Pb–Te system [47,48].

Phonons may be scattered by three important mechanisms:

(i) Collision of a phonon with other phonons (phonon–phonon interaction).
(ii) Collision of a phonon with imperfections in the lattice, e.g. impurities, dislocations (phonon–lattice disorder interaction).
(iii) Collision of a phonon with boundaries.

The first two scattering mechanisms become ineffective at very low temperature ($T < 10$ K). In the low temperature region, the third scattering mechanism (scattering of phonons at the boundaries) becomes the predominant mechanism, because the wave length of the phonons are very long comparable to the size of the relative grains. The mean free path here is $l \sim D$, where D is roughly equal to the grain diameter and is therefore independent of temperature [43].

At low temperature ($T \ll \theta_D$, where θ_D is the Debye temperature), the lattice thermal conductivity varies with T^3 due to the dependence of the specific heat on T^3 in this range of temperature [44], as seen from the following expression for C_v:

$$C_V = \frac{(12\pi^2)}{5} R \left(\frac{T}{\theta_D}\right)^3, \tag{35}$$

where R is the gas constant.

It is possible to express the different relaxation times in terms of the reduced phonon frequency x ($= \hbar\omega/kT$) as:

(1) For the 3-phonon, U-process, the relaxation time τ_U is given by

$$\tau_U = \frac{1}{a_U x^2} \tag{36}$$

and for the 3-phonon, N-process, the relaxation time τ_N is given by

$$\tau_N = \frac{x^2}{a_N} = \frac{1}{k_0 a_U x^2}, \tag{37}$$

where $k_0 = a_N/a_U$ represents the relative strength of N–U processes.

(2) For the boundary scattering, the relaxation time may be given by [45]

$$\tau_B = L/V, \tag{38}$$

where L is the Casimir length and is given by

$$L = \text{Casimir length} \times F$$
$$= 3.47 \times 10^3 \, dpQ^{-1/3}v^{-1}F,$$

where d is the crystal diameter, p the dimensionless parameter (~ 1.4), Q the specific heat constant, v the sound velocity, and F the correction factor for the finite length of the specimen.

(3) In case of point defect scattering, the relaxation time is given by [46]

$$\tau_D = \frac{1}{a_D x^4}, \tag{39}$$

where a_D as shown by Klemens [46] is given by

$$a_D = \left(\frac{v\Gamma\Omega_0}{4\pi}\right)\left(\frac{kT}{\hbar v}\right)^4,$$

where Ω_0 is the volume per atom and Γ a disorder parameter

2.4.5.1. The lattice thermal conductivity λ_L. The lattice thermal conductivity λ_L can be expressed in terms of three parameters A, B, and C. A depends upon disorder (alloying), B is a measure of the strength of phonon–electron/hole coupling (doping), and C is usually expressed in terms of a parameter D, which is inversely proportional to grain size L. C and D are related by [17]

$$D = CT, \tag{41}$$

where T is the temperature. $A = 0$ corresponds to unalloyed material with no disorder present, $B = 0$ corresponds to undoped material, and $C = 0$ corresponds to single crystal material.

It was shown that, in general [17]

$$\lambda_L(A, B, C = 0) = \lambda_{Lsingle} \tag{42}$$

represents the lattice thermal conductivity of a doped single crystal alloy.

Graphs of $\lambda_L/\lambda_{Lsingle}$ at room temperature for unalloyed PbTe ($A = 0$) and highly disordered alloys of PbTe ($A = 5$) are shown in Fig. 19 as a function of grain size and level of doping.

2.4.5.2. The electronic thermal conductivity λ_e. The electronic thermal conductivity λ_e is expressed

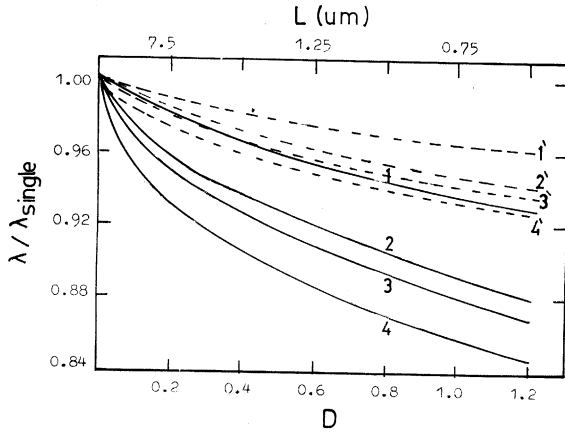Fig. 19. Plot of $\lambda_L/\lambda_{Lsingle}$ for unalloyed (dashed lines) and highly disordered alloys (solid lines) of n-type PbTe at 300 K as a function of grain size and level of doping. $k_0 = 1.0$, $A = 0$; curves: $1,1'$—$B = 0.05$; $2,2'$—$B = 0.010$; $3,3'$—$B = 0.005$; and $4,4'$—$B = 0$ [41].

as [1,16]

$$\lambda_e = L'(k/e)^2 \sigma T, \tag{43}$$

where L' is the dimensionless Lorenz factor, and $L'(k/e)^2$ is the Lorenz number L.

When using the classical statistics, the Lorenz factor is given by [16]

$$L' = \left(\tfrac{5}{2} + s\right), \tag{44}$$

but when Fermi–Dirac statistics are used, L' is expressed as

$$L' = \frac{(s+\tfrac{1}{2})F_{s+5/2}(\xi)}{(s+\tfrac{3}{2})F_{s+1/2}(\xi)} - \left[\frac{(s+\tfrac{5}{2})F_{s+3/2}(\xi)}{(s+\tfrac{3}{2})F_{s+1/2}(\xi)}\right]^2, \tag{45}$$

where $F(\xi)$ is the Fermi integral defined by

$$F_s(\xi) = \int_0^\infty \frac{x^s \, \mathrm{d}x}{e^{x-\xi} + 1} \tag{46}$$

and ξ is the reduced Fermi energy, and s is a scattering parameter that depends upon the scattering mechanism.

In order to show the dependence of λ_L on grain size (L), the grain size is classified by using a set of microsieves and compacts of grain sizes $10 < L < 20\,\mu m$ and $L \sim 1\,\mu m$ were used [34,59] in addition to single crystal to compare with.

2.4.6. Mixed scattering

In real systems, two or more scattering mechanisms usually operate. The contribution of each type of the scattering mechanism varies strongly with temperature and impurity concentration. In heavily doped semiconductors, normally at least two scattering mechanisms must be considered:

(i) scattering by ions and acoustic phonons, or
(ii) scattering by ions and optical phonons.

In covalent semiconductors scattering of carriers occurs by ions and acoustic phonons while in polar semiconductors, carriers are scattered by ions and optical phonons. In case of mixed scattering when acoustic phonons and impurity scattering act simultaneously, each has a relaxation time defined by [16,42]

$$\tau_{ac} = \tau_{oL}\eta^{-1/2}, \tag{47}$$

$$\tau_{imp} = \tau_{oi}\eta^{3/2}, \tag{48}$$

and the combined relaxation time τ is given by

$$\frac{1}{\tau} = \sum_{i=1}^{i=2} \frac{1}{\tau_i}. \tag{49}$$

So the combined relaxation time τ can be written as

$$\tau = \tau_{oL}\eta^{3/2}/(\eta^2 + b^2), \tag{50}$$

where $b^2 \; (= \tau_{oL}/\tau_{oi})$ is a measure of the relative strength of the ionized impurity scattering and lattice scattering, and $\eta = E/kT$ is the reduced carrier energy.

Fig. 20 shows the calculated values of λ_e of n-type PbTe as a function of carrier concentration (n) and temperature (T) assuming that electrons are scattered by acoustic phonons [41]. At $n > 10^{24}\,m^{-3}$, λ_e becomes comparable with λ_L and increases rapidly with a further increase in carrier concentration. Assuming a temperature dependence of $1/T$ for λ_L, the total thermal conductivity λ_t is obtained as a function of n and T as shown in Fig. 21. Fig. 22 shows the total thermal conductivity of n-type PbTe as a function of temperature for two different carrier concentrations: $n = 5 \times 10^{24}$ and $10^{25}\,m^{-3}$ [41].
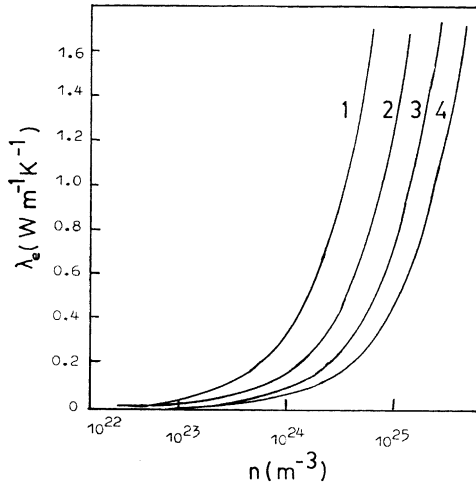
Fig. 20. Electronic thermal conductivity λ_e for n-PbTe as a function of carrier concentration and temperature (acoustic scattering and non-parabolic bands). Curves 1, 2, 3, and 4 correspond to temperatures of 300, 450, 600, and 750 K, respectively [41].
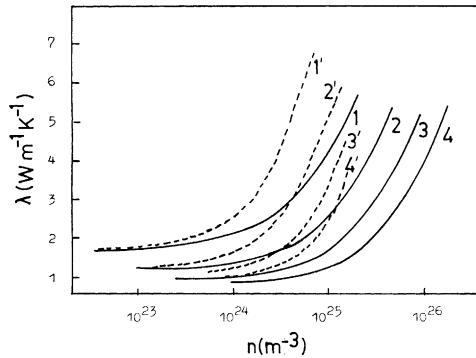

Fig. 21. Total thermal conductivity λ_t as a function of carrier concentration and temperature (acoustic scattering). 1,1′— 300 K; 2,2′—450 K; 3,3′—600 K; and 4,4′—750 K (dashed lines: parabolic bands; solid lines: non-parabolic bands [41]).

Fig. 22. Total thermal conductivity λ_t as a function of temperature. 1,1′—$5 \times 10^{24} \, \text{m}^{-3}$; 2,2′—$10^{25} \, \text{m}^{-3}$; and 1′,2′ include scattering of electrons by polar optical modes along with the acoustic modes. Experimental points: 5×10^{24} and $10^{25} \, \text{m}^{-3}$ [41].

Scattering of phonons by free electrons was taken into account when calculating λ_L contribution to Fig. 22.

From the previous figures, it is concluded that the effect of the acoustic and polar optical scattering modes and the effect of non-parabolic energy bands should be taken into consideration in the calculations of λ_e.

This review article gives a brief and concentrated material about lead telluride as a useful thermoelectric material for power generation. For more details, it is advised to refer to the given references in every section.

At $n \sim 10^{25} \, \text{m}^{-3}$, λ_e contribution to λ_t becomes dominant, and contribution to polar optical mode scattering should also be included in the calculation of λ_e. In Fig. 22 curves 1 and 2 correspond to acoustic phonon scattering and the effect of non-parabolic energy bands; curves 1′ and 2′ are of the total thermal conductivity λ_t with λ_e is given by [41]

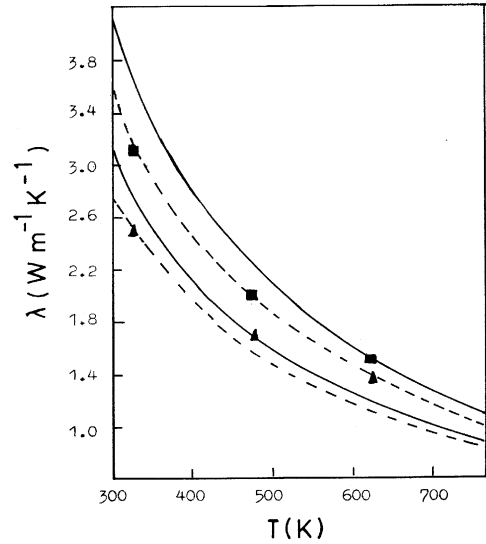$$\lambda_e^{-1} = \lambda_{e,\text{acous.}}^{-1} + \lambda_{e,\text{optic.}}^{-1}. \tag{51}$$

References

[1] H.J. Goldsmid, Applications of Thermoelectricity, Methuen, London, 1960.
[2] A.F. Ioffe, Semiconductor Thermoelements and Thermo-electric Cooling, Info-search, London, 1956.
[3] J.P. Angello, G.T. Prysinger, Intersociety Energy Conversion Engineering Conference, IEEE, USA, 1968, p. 986.
[4] G. Guazzoni, Intersociety Energy Conversion, IEEE, USA, 1970, p. 136.

[5] V. Raag, R.E. Berlin, Adv. Energy Convers. 8 (1968) 161.

[6] D.M. Rowe, Proceedings of the IEEE, USA, 1978, p. 1113.

[7] D.K.C. MacDonald, Thermoelectricity: an Introduction to the Principles, Wiley, New York, 1962.

[8] R.R. Heikes, R.W. Ure, Thermoelectricity: Science and Engineering, Inter-science, London, 1961.

[9] M. Telres, J. Appl. Phys. 25 (1954) 765.

[10] F.D. Rosi, E.F. Hockings, N.E. Lindeblad, RCA Rev. 22 (1961) 82.

[11] F.D. Rosi, Solid State Electron. 11 (1968) 833.

[12] D.A. Wright, Metall. Rev. 15 (1970) 147.

[13] C.M. Bhandari, D.M. Rowe, Contemp. Phys. 21 (1980) 219.

[14] V.S. Shukla, Ph.D. Thesis, University of Wales, 1980.

[15] V. Raag, Proceedings of the 93rd Winter Meeting of ASME, 30th November, 1972, p. 144.

[16] D.M. Rowe, C.M. Bhandari, Modern Thermoelectrics, Holt, London, 1983.

[17] C. Kittle, Introduction to Solid State Physics, Wiley, New York, 1971.

[18] A.F. Ioffe, Dok. Akad. Nauk SSSR 106 (1956) 981.

[19] C.M. Bhandari, D.M. Rowe, Energy Convers. Manag. 20 (1980) 113.

[20] C.M. Bhandari, D.M. Rowe, J. Phys. C 11 (1978) 1787.

[21] H.J. Goldsmid, A.W. Penn, Phys. Lett. 27A (1968) 523.

[22] J.E. Parrott, J. Phys. C 2 (1969) 147.

[23] C.M. Bhandari, D.M. Rowe, J. Phys. D 18 (1985) 873.

[24] Yu.I. Ravich, B.A. Efimova, I.A. Sminova, Plenum, New York, 1970.

[25] Yu.I. Ravich, B.A. Efimova, V.I. Tamarchenko, Phys. Stat. Sol. B 43 (1971) 11.

[26] W.W. Scanlon, Polar Semiconductors, Solid State Physics, Advances in Research and Applications, Academic Press, New York, 1959.

[27] V. Raag, V.C. Truscello, Proceedings of the ASME Winter Meeting, New York, 1972, p. 27.

[28] G.L. Bennet, J.J. Lombardo, B.J. Rock, J. Astronau. Sci. 29 (1981) 321.

[29] I. Stambler, Space Aeronau. 9 (1962) 69.

[30] C. Wood, Rep. Prog. Phys. 51 (1988) 459.

[31] H.R. Meddins, J.E. Parrott, Phys. Chem. Solids 9 (1976) 1263.

[32] J.W. Killian, Intersociety Energy Conversion Engineering Conference, Record, 13–17 August, 1968.

[33] D.R. Field, G.W. Bunde, Space and Defence Products Department, 3M Company, St. Paul, MN, USA, 1968, p. 425.

[34] Z.H.D. Al-Masri, Ph.D. Thesis, University of Wales, 1991.

[35] R.S. Reylek, E.F. Hampl, J.D. Hinderman, R.L. Smith, D.A. Wald, IEEE, USA, 1976, p. 1599.

[36] J.C. Bass, N.B. Elsner, Proceedings of the Third International Conference on Thermoelectric Energy Conversion, University of Texas, Arlington, 1980, p. 8.

[37] C.M. Bhandari, D.M. Rowe, J. Appl. Phys. 16 (1983) L75.

[38] T.L. Kovalchik, Iu.P. Maslakovets, Sov. Phys. Tech. Phys. 1 (1957) 2337.

[39] L.D. Borisova, Phys. Stat. Sol. A 53 (1979) K19.

[40] P.G. Rustomov, M.A. Alidzhanor, C.H.I. Abilov, Phys. Stat. Sol. A 12 (1972) K103.

[41] C.M. Bhandari, D.M. Rowe, Appl. Phys. A 37 (1985) 175.

[42] V.I. Fistul, Heavily Doped Semiconductors, Plenum, New York, 1969.

[43] N. Savvides, H.J. Goldsmid, J. Phys. C 13 (1980) 4671.

[44] M.A. Omar, Elementary Solid State Physics, Addison-Wesley Publishing Company Inc., London, 1975.

[45] R. Berman, J.C.F. Brock, Proc. Roy. Soc. A 289 (1965) 46.

[46] P.G. Klemens, Proc. Phys. Soc. A 68 (1955) 1113.

[47] F.A. Shunk, Constituent of Binary Alloys, McGraw Hill, New York, 1969.

[48] R.F. Brebrick, R.S. Allgaier, J. Chem. Phys. 32 (1960) 1926.

[49] C.M. Bhandari, D.M. Rowe, Thermal Conduction in Semiconductors, Wiley Eastern Ltd., New Delhi, 1988.

[50] S.P. Yordanov, Bulgar. J. Phys. 17 (1990) 6.

[51] S.P. Yordanov, Bulgar. J. Phys. 18 (1991) 15.

[52] P.K. Parries, D. Mukherjee, C.A. Hogarth, Phys. Stat. Sol. A 152 (1995) 461.

[53] A.Y. Ueta, G. Springholz, F. Schinagl, G. Marschner, G. Beauer, Thin Soild Films 306 (1997) 321.

[54] A.V. Wagner, R.J. Foreman, J.C. Farmer, T.W. Barbee Jr., Material Research Society, Philadelphia, PA, USA, 1997, p. 465.

[55] L. Chen, T. YuGoto, R.Tu.T. Hirai, IEEE, USA, 1998, p. 539.

[56] O. Ito, Seo Won-Son, K.Kounoto, J. Mater. Res. 14 (1999) 209.

[57] D.M. Rowe, C.M. Bhandari, Z.H. Dughaish, Proceedings of the First Asian Thermo-physical Properties Conference, Beijin, China, 1986, p. 718

[58] Z.H. Dughaish, D.M. Rowe, J. King Saud Univ. (Sci.) 13 (2001) 23.

[59] Z.H. Dughaish, Physica B 299 (2001) 94.

[60] G. Chen, Int. J. Thermal Sci. 39 (2000) 471.

[61] D.Y. Yao, C.J. Kim, G. Chen, ASME International Mechanical Engineering Congress and Exchange, 5–10 November, Orland, FL, 2000.

[62] A. Shakouri, J.E. Bowers, Appl. Phys. Lett. 71 (1997) 1234.

[63] X. Fan, G. Zeng, C. LaBounty, J.E. Bowers, E. Croke, C.C. Ahh, S. Huxtable, A. Mahumdar, A. Shakbouri, Appl. Phys. Lett. 78 (11) (2001) 1580.

[64] L.D. Hicks, M.S. Dresselhaus, Phys. Rev. B 47 (19) (1993) 12727.

[65] L.D. Hicks, M.S. Dresselhaus, Phys. Rev. B 47 (19) (1993) 16631.

[66] T.C. Harman, P.L. Spears, M.J. Manfra, J. Electron. Mater. 25 (7) (1996) 1121.

[67] H. Beyer, Proceedings of the 18th International Conference on Thermoelectrics, Baltimore, USA, 1999, p. 687.

[68] P. Hyldgaard, G.D. Mahan, Phys. Rev. B 56 (17) (1997) 10754.

[69] A. Balandin, K.L. Wang, Phys. Rev. B 58 (1998) 1544.

[70] A. Balandin, K.L. Wang, J. Appl. Phys. 84 (1998) 6149.

[71] G. Dresselhaus, M.S. Dresselhaus, Z. Zhang, X. Sun, J.Y. Ying, G. Chen, in: K. Koumoto (Ed.), Proceedings of the 17th International Conference on Thermoelectrics, The Institute of Electrical and Electronics Engineers, Inc., Piscataway, NJ, 1998, p. 12.

[72] M.S. Dresselhaus, G. Dresselhaus, X. Sun, Z. Zhang, S.B. Cronin, T. Koga, J.Y. Ying, G. Chen, Microscale Thermophys. Eng. 3 (2) (1999) 89.

[73] T. Kong, S.B. Cronin, M.S. Dresselhaus, Appl. Phys. Lett. 77 (2000) 1490.

[74] A. Khitun, A. Balandin, K.L. Wang, G. Chen, Physica E 8 (2000) 13.

[75] D.M. Rowe, C.M. Bhandari, in: D.M. Rowe (Ed.), CRC Handbook of Thermoelectrics, CRC Press, Boca Raton, FL, 1995, ISBN: 0849301467.